JAAS

PAPER

View Article Online
View Journal | View Issue

Cite this: J. Anal. At. Spectrom., 2021, 36, 1996

Quantitative measurement of the mixture ratio for ADN-based liquid propellants using laser-induced breakdown spectroscopy

Fangyi Wang,[ab] Shaohua Zhang,[*a] Xilong Yu,[ab] Xin Lin,[a] Jing Li[cd] and Yan Liu[cd]

Laser-induced breakdown spectroscopy (LIBS) experiments were carried out with an ammonium dinitramide (ADN)-based propellant to measure its distribution, that is the mixture ratio, in an inert atmosphere. A heating sampler was developed to produce a premixed sample with a known mixture ratio and this was connected to a chamber that had been designed to simulate the space propulsion environment. Determining the time window for the acquisition and saturation threshold of LIBS were the main motivations to investigate the effective lifetimes of atomic spectral lines and the effect of laser energy on the emission ratio. From the spectroscopic analysis, it was found that the ratio of the intensities of H (656.3 nm), O (777 nm) and N (746.8 nm) over Ar (738.4 nm) increased monotonically with the mixture ratio in the range of 0–0.06. A series of propellant/Ar mixtures with a pressure in the region of 40–100 kPa were used to obtain a linear correlation between the intensity ratio of LIBS spectra and the local mixture ratio. It was observed that the logarithm of the slope of the lines also showed a linear correlation with the pressure. Considering that the current method was applied by necessity with the given pressure, the local pressure was studied based on its dependence on the full width at half maximum (FWHM) of H and Ar spectral lines. Consequently, the emission ratios of H/Ar, O/Ar and N/Ar were utilized as a diagnostic tool to obtain the distribution of the propellant in the inert atmosphere. The LIBS-based results not only provide fundamental data for the on-line measurements of ADN-based thrusters, but also hold promise for promoting the application of LIBS in the field of energetic ionic liquids.

Received 31st May 2021
Accepted 20th July 2021

DOI: 10.1039/d1ja00186h

rsc.li/jaas

1. Introduction

Over the past decades, energetic ionic liquids have become a new innovative research direction in the field of space chemical propulsion with a priority towards enabling technology for novel interplanetary vehicles and launchers. As one of the most promising monopropellants to replace hydrazine, which is currently the most widely used, ammonium dinitramide ($NH_4N(NO_2)_2$, ADN)-based liquid monopropellants have attracted much attention since ADN was first synthesized in 1971. The detailed properties of ADN are summarized in Table 1, but the main characteristics include its low toxicity and environmental friendliness,[1,2] which suggest that ADN-based liquid monopropellants can effectively match the in-space mission needs and help solve the drawbacks caused by hydrazine, such as its complex handling and testing procedures.

In general, ADN acts as a soluble oxidizer in ADN-based propellants, which also contain ionic fuel and water (and stabilizer sometimes). As a non-toxic and pollution-free monopropellant, ADN-based liquid propellants are already applied in the field of micro-thrusters with a solid catalyst.[3–5] The technical possibility and energy supply capability have also been verified during the thruster's launching and flying in orbit. However, there is a fatal problem in the current catalytic ignition that the catalyst sinters, reduces and then deactivates in environments with an adiabatic flame temperature. Many other ignition

Table 1 Basic properties of ADN

Density at 20 °C	1.81 g cm^{-3}
Initial decomposed temperature	160 °C
Melting point	91 °C
Molecular weight	124.056 g mol^{-1}
Enthalpy of melting	140 J g^{-1}
Oxygen balance	+25.79%
Heat of formation	−148 kJ mol^{-1}

[a]State Key Laboratory of High Temperature Gas Dynamics, Institute of Mechanics, Chinese Academy of Sciences, Beijing 100190, China. E-mail: shzh@imech.ac.cn
[b]School of Engineering Science, University of Chinese Academy of Sciences, Beijing 100049, China
[c]Key Laboratory of Advanced Energy and Power, Institute of Engineering Thermophysics, Chinese Academy of Sciences, Beijing 100190, China
[d]Research Centre for Clean Energy and Power, Chinese Academy of Sciences, Lianyungang, Jiangsu 22046, China

approaches, especially the plasma-assisted,[6–10] have been utilized in recent years to break this restriction. Most studies have used an inert gas atmosphere due to its low reactivity, which makes it an ideal candidate given the complicated reactions already caused by this mixture propellant. There are some structural improvements proposed to initiate combustion or stabilize the flame better. For the reason of a thorough reaction, a swirling gas supply system, porous propellant supply system and larger-scale discharge electrodes have been adopted to enlarge the contact area between the plasma and propellant as well as to prolong the reaction time, which have demonstrated that mixing the propellant completely is bound to increase the possibility of a successful ignition. It can be concluded that the decisive factor affecting the experimental results is the distribution of the propellant in the inert atmosphere. Therefore, exploring the mixture ratio of the propellant and carrier gas is essential during the thruster operation to evaluate the efficiency of the propellant as well as to improve the propulsive performance. Unfortunately, the distributions of the liquid propellant or its reaction intermediates are still unclear due to the lack of available information from accurate measurements during the procedures of discharge, laser ablation and plasma interaction. Hence, quantitative optical diagnostic techniques need to be developed with an ability to perform high sensitivity and on-line measurements.

As a non-intrusive diagnostic technique, laser-induced breakdown spectroscopy (LIBS) allows measuring a mixture composition, proportion and temperature.[11–14] A focused pulsed laser beam utilized, leading to the breakdown and the formation of laser-induced plasma. The elemental composition of the test samples in any state can be identified based on their fingerprint spectral lines collected by a spectrometer equipped with an intensified charged couple device (ICCD) detector, while the concentration of such elements can be quantified from the intensity of the spectral lines. It is worth noting that the relative intensity of the spectral emission lines is often employed to obtain quantitative information on the atomic species considering the effects of the instrument parameters and the subtle variations of laser energy. LIBS can rapidly analyse samples *in situ*, no matter gases or liquids or solids, with minimal sample preparation. It also has the potential for simultaneous multi-elemental analysis with simple equipment and the capability to measure in extreme conditions.[15–17] These advantages make the LIBS technique an attractive tool to measure the mixture ratio, which is a challenging yet essential task in the field of combustion diagnostics.

Recently, the LIBS technique has been extensively applied to determine the equivalence ratio[18–21] in the field of aerospace propellants, mostly taking solid propellants as the target.[22–27] The sensitivity of analysis in the bulk liquid remains a key issue because most of the plasma energy is lost in vaporization of the surrounding liquid and in the generation of a shockwave and cavitation bubbles accompanying the breakdown.[28] However, some researches still focused on liquid samples due to the huge potential that LIBS offers in a number of applications. As a method most commonly used in the liquid phase, surface LIBS is quick and straightforward without needing pre-treatment of the sample. Mousavi *et al.*[29] studied the plasma emission of liquid benzene and carbon disulfide based on surface LIBS in air, but found the emission signal was affected by the surrounding atmosphere. From the point of view of the actual combustion conditions, the breakdown point cannot be always guaranteed in the surface of a droplet. Hence many researchers have taken the vapour as the object. For instance, Nozari *et al.*[30] applied LIBS in a quartz tube to characterize some organic vapours at atmospheric pressure. However, this is not suitable for the detection of ADN-based propellants because its low volatility and the chemical reactions that may occur between the components during evaporation. In addition to the lab-scale chamber, Stützer *et al.*[31] applied LIBS in hot firing tests at the European research test bench P8 with hydrogen or methane in the gas phase and oxygen in the liquid phase, which were injected in to the bench in a non-premixed way. The technical feasibility was demonstrated during the practical application, admittedly, but differences between the liquid oxygen and multicomponent propellant must be considered. Examination of the aforementioned literature suggests that the mixture ratio is a crucial parameter to assess the ignition

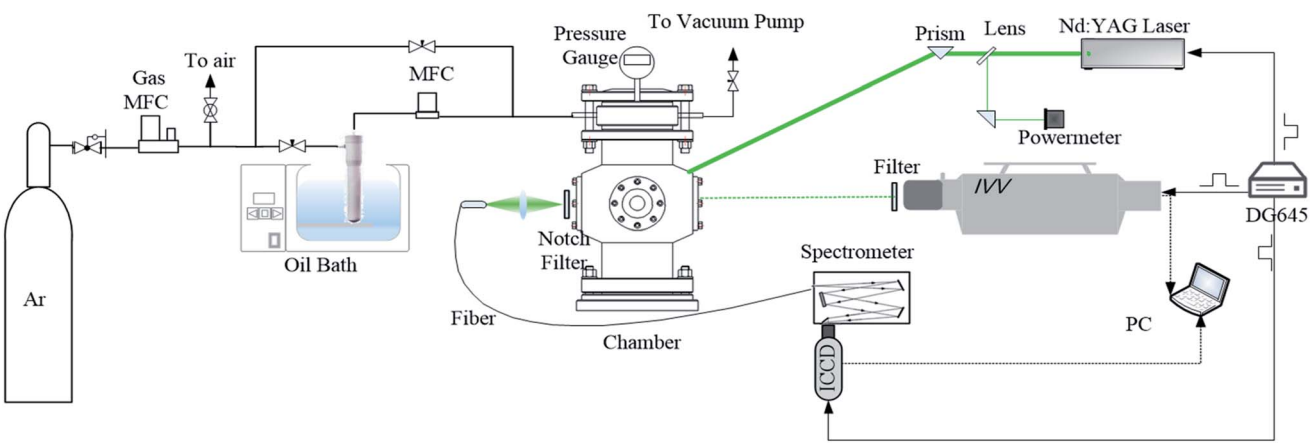

Fig. 1 Experimental set-up.

possibility. After all, an accumulation of the propellant close to the wall and a short duration of premixing would mean the propulsion system might be unable to start-up.

In the meantime, it can be seen that most studies rarely involve ADN-based liquid propellants, which possess complicated physicochemical properties due to the many components they contain. There are still many challenges in carrying out LIBS experiments, despite the strong engineering application background of ADN-based liquid propellants as mentioned above. In order to achieve a practical propulsion system, the state of this propellant should be set as small droplets or in the gasification state. Furthermore, the mixture ratio measured by LIBS could be utilized in the combustion chamber or at the outlet of the nozzle to evaluate the uniform area of the flow field. Owing to these issues, the use of the LIBS technique in the field of developing ADN-based propellants under propulsion circumstances remains unproven, and given the corresponding severe changes of the propellant concentrations both temporally and locally, further work is needed to: (i) establish a set-up for a premixed propellant and carrier gas, (ii) develop calibration correlations spanning a wide range of working conditions, (iii) investigate the precision of the results.

The present work was carried out in a chamber with a constant volume for simulating the aerospace microthruster environment. A heating sampler was designed to produce premixed samples and to obtain a precise mass flow rate of the ADN-based propellant. In addition, to discuss assessing the ignition possibility by ultra-high-speed imaging, this paper explores the relevant set-up of LIBS and the calibration lines between the intensity ratio and mixture ratio. The experimental data possess great significance to improve the performance of propulsion systems, whereby the measurements could also be references for the on-line diagnostics of propulsion system based on ADN-based propellants, as well as for other energetic ionic liquids.

2. Experimental

The experimental set-up for the LIBS-based mixture ratio measurements is shown in Fig. 1, and was composed of three parts, as described in the following.

2.1. Constant volume chamber and sample supplying system

A stainless-steel flow chamber was designed for premixing the samples for the LIBS experiments, as shown in Fig. 1. The stainless chamber was equipped with optical accessible quartz windows with a transmission range of 200–2000 nm on all four sides. The chamber pressure could be adjusted in the 0–1 bar range, as monitored by a high-precision pressure sensor.

Pure argon (99.999%) was introduced into the chamber and monitored by a mass flow controller (CS200, SevenStar). Then the argon gas entered the Teflon-lined sampler with a 75 mL volume and which contained the ADN-based liquid propellant. The detailed structure of the sampler is displayed in Fig. 2. The composition of the ADN-based propellant sample applied in this experiment is listed in Table 2. The sampler was placed in an oil bath assembly, which could be heated up to 300 °C with dimethyl silicone oil inside. A premixed sample containing a variable ratio of the vaporized propellant and argon supplied from the sampler was slowly passed through the chamber. A stable chamber pressure and dynamic balance of the premixed sample were achieved through precise adjustment of the input and by evacuation during the experiment.

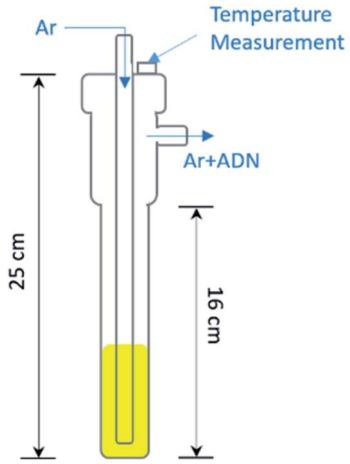

Fig. 2 Detailed structure of the sampler containing the propellant.

Table 2 Composition of the ADN-based liquid propellant

Component	Proportion	Role
$NH_4N(NO_2)_2$	63%	Oxidizer
CH_3OH	11%	Fuel
H_2O	26%	Solvent

It was noteworthy that a translucent pipe made of Teflon was used to connect the exit of the sampler and the entrance of the chamber and this was kept as shorten as possible, making it more convenient to check and avoid the accumulation on the inner shell of the pipe. Besides, the application of the thermal insulation belt with a self-limiting temperature in the exterior pipe shell played a double-handed role in also maintaining the identical state of the propellant from the sampler to the chamber. A temperature measurement port was designed to record the temperature of the ADN-based liquid propellant. A temperature calibration curve was obtained in advance to observe the correlation between the setting temperature of the oil bath assembly and the internal temperature of propellant. The latter was used as one of the normative variables during the experiment.

The preheating temperature corresponded to the application background of the ADN-based liquid propellant as mentioned above. Accordingly, the temperature of the oil bath assembly was set in the range of 30–100 °C, which is closer to the actual working condition. The flow rate of argon was set at 0.2 L min^{-1}, while that of the propellant varied in the range of 0.28–2.62 g

h^{-1}, corresponding to the mixture ratio in the 0.006–0.057 region based on eqn (1):

$$r = \frac{M_{Ar}}{M_{propellant}} \frac{F_{propellant}}{F_{Ar}} \quad (1)$$

where M_{Ar} is the relative atomic mass of Ar, $M_{propellant}$ is the relative molecular mass calculated by the proportion of components, and F represents the mass flow rate of argon gas or the propellant. It may be noticed that the mass flow rate of the propellant ($F_{propellant}$) was obtained by the weight method, which is commonly used in the space sector.

2.2. LIBS set-up

The LIBS signals of the ADN-based propellant/argon mixture were generated from the excited atoms in the micro plasma, which were created by focusing the second harmonic output of a Nd:YAG laser (Quanta-Ray 190, Spectra-Physics) at 532 nm with a output frequency of 10 Hz. The single pulse energy of the excited laser was set as 140 mJ (±5 mJ), unless otherwise specified. A quartz lens with a focal length of 125 mm was applied to focus the laser beam. The emission of the plasma was collected by a 30 mm focal length quartz lens in the perpendicular direction of the laser. Then, the LIBS signals were focused into the fibre, which was positioned at the outer surface of a side optical window with a diameter of 1 mm, and transmitted into the spectrometer (HRS-500, Princeton Instruments, Spectral range: 200–900 nm) with a 30 μm input slit. An ICCD camera (PI-MAX4, Princeton Instruments) equipped with a spectrometer was utilized, whose delay and width of the gate were varied in the tests. The LIBS signals during testing were averaged three times to obtain a good signal-to-noise ratio (S/N).

The grating efficiency of the spectrometer was calibrated by a NIST standard traceable tungsten halogen lamp (63976, Oriel Instruments), while wavelength calibration of the system proceeded with a standard Hg–Ar lamp.

2.3. Ultrahigh-speed imaging set-up

Image visualization was achieved by an ultrahigh-speed framing camera (Ultra UHSi 12/24, Invisible Vision Ltd), which was set perpendicular to the laser. The camera was set up with fully independent programmable exposures and delays down to 5 ns and frame rates to 200M fps to visualize the morphology and continuum radiation of the plasma. A camera lens (AF-S NIKKOR 50 MM F/1.8G) was equipped since the spectral window of this camera was in the visible range. The output of the camera was analysed with a computer data acquisition system.

It is believed that a combination of imaging devices and optical filters with a narrow transmittance window for accurate wavelength selection offers a cost-effective recording method for analysing selective spectral images. Hence, with a bandpass filter (central wavelength of 600 nm with 80 nm half-band width, GCC-203004), the continuum radiation was observed without interference of the spectral signal owing to the strong groups of emission lines from the Ar ions (400–500 nm) and Ar atoms (700–850 nm).

Experimental synchronization was controlled through a multi-channel digital delay pulse generator (DG645, Stanford Research System). It was noted that the time scale in the following text was unified, which took the laser arrival as time zero.

3. Results and discussion

3.1 Evolution of plasma in the initial stage

Understanding the evolution of plasma at the initial stage, when the continuum radiation plays a dominant role, can be extremely helpful to monitor the conditions of the laser-induced plasma and to correlate the plasma to the ablation mechanism. The following discussion is based on the continuum radiation and temporal shape of the spark in the laser-induced plasma.

As Fig. 3 shows, the spectrum was mainly composed of a strong continuum emission and superimposed ionic spectral lines once the laser-induced plasma appeared. Then, the intensity of the ionic spectral lines gradually decreased due to the expansion, cooling effect and the recombination reactions within the plasma. Meanwhile, the intensities of the atomic

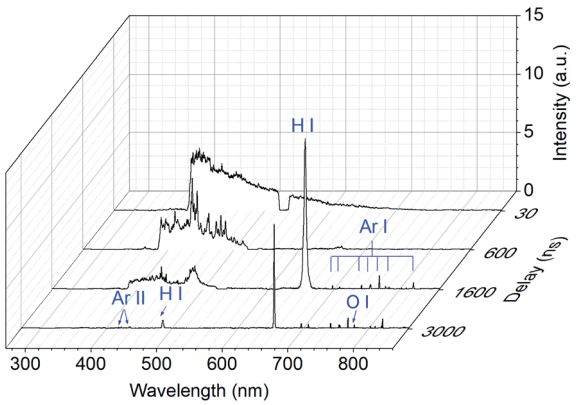

Fig. 3 Corrected spectra with different delays.

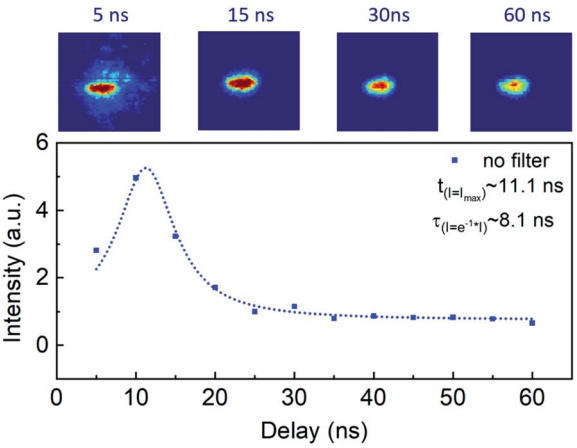

Fig. 4 Ultrahigh-speed imaging and intensity curve of the emission signal (no filter).

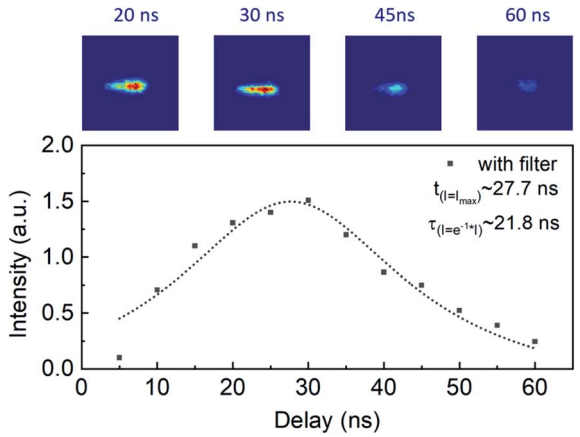

Fig. 5 Ultrahigh-speed imaging and intensity curve of the continuum radiation signal (with filter).

spectral lines increased. It could be inferred that the atomic spectral lines under the current experimental conditions mainly came from the transitions of excited atoms formed by the recombination of ions and free electrons based on the temporal difference between the peak intensities of the atomic lines and ion lines. It could be noticed that the drop around 532 nm was caused by a notch in the filter.

The wavelength range from 560 nm to 640 nm in Fig. 3 was selected using a bandpass filter to represent the continuum radiation, as discussed earlier. A special set-up for ultrahigh-speed imaging was applied to obtain the intensity of the continuum radiation of the laser-induced plasma in this experiment. Fig. 4 and 5 show the sequences for the temporal development of the laser-induced plasma and its continuum radiation with a total pressure, that is, vapor from ADN-based propellant and argon gas, of 40 kPa and laser energy of 140 mJ per pulse, respectively. The acquisition of data with an exposed gate width of 5 ns generally starts when the laser pulse arrives in the chamber, as monitored by a silicon photodiode. The first set of images in Fig. 4 display the position of the spark, indicating a stable flow field in the chamber. The laser beam in this experiment showed a Gauss profile, which led to the images in Fig. 5, which show that the continuum radiation has a higher value in the location nearer to the centre line of the laser incident direction. Although a decreasing trend could be clearly observed in both sets of images, quantitative analysis was proposed to explore the ignition possibility.

The intensity of the signal zone was calculated by summing the value of each pixel and displaying this against time as intensity curves in Fig. 4 and 5. The maximum laser intensity and continuum radiation intensity appeared at 11.1 ns and 27.7 ns, respectively. Exponential decay fitting was used to obtain the relaxation time of the laser-induced plasma (no filter) and of the continuum radiation (with filter), which were 8.1 ns and 21.8 ns. The intensity of the continuum radiation with the bandpass filter decreased more slowly in comparison to those observed without a filter. It is worth noting that it was not possible to distinguish all the continuum radiation from the spectra till the delay of around 1 μs, as evidenced by the flame kernel not being produced in all working conditions as the intensity could last for 100 μs (ref. 32) with the chemiluminescence generated in the flame kernel. This would usually be observed in a successful ignition.

In the local thermodynamic equilibrium state, the continuum radiation in plasma is a coupled result of Bremsstrahlung, recombination, and black-body radiation usually. It is shown that Bremsstrahlung and black-body radiation increased with a higher electron temperature, while the recombination radiation presented the opposite effect based on the following:[33,34]

$$P_{\mathrm{br}} \propto \frac{1}{\lambda^2 T_{\mathrm{e}}^{1/2}} \exp\left(-\frac{1}{T_{\mathrm{e}}}\right) \quad (2)$$

$$P_{\mathrm{re}} \propto \frac{1}{(T_{\mathrm{e}})^{3/2}} \exp\left(-\frac{1}{T_{\mathrm{e}}\lambda}\right) \quad (3)$$

$$P_{\mathrm{bl}} \propto \frac{1}{\lambda^5 \exp\left(\frac{1}{T_{\mathrm{e}}\lambda} - 1\right)} \quad (4)$$

where P_{br}, P_{re}, P_{bl} is the irradiance of Bremsstrahlung, recombination and black-body radiation, respectively, T_e is the electron temperature, and λ is the wavelength.

Therefore, the Bremsstrahlung and black-body radiation play dominant roles for over tens of nanoseconds after the

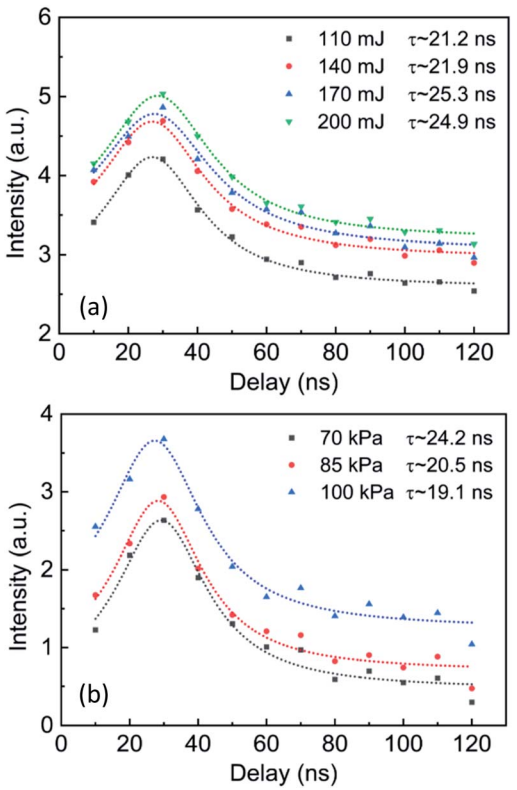

Fig. 6 Relative intensities of the continuum radiation as a function of the: (a) laser pulse energy, (b) gas pressure.

breakdown with a high electron temperature. With a delay of 30 ns, as shown in Fig. 3, the intensity of the short waveband is much higher than the long waveband in the spectrum according to eqn (2)–(4), which was due to the atoms and molecules produced by recombination reaction possessing a lower excited energy. The recombination reaction becomes a more decisive factor after that due to its compensation effect on the collisional process in plasma. The intensity of the continuum radiation declined due to the combined effect of the Bremsstrahlung and recombination reaction.

The intensity of continuum radiation depends on, in particular, the chamber pressure and electron temperature among many factors. Hence, the impact of laser energy and gas pressure on the relative intensities of the continuum radiation were investigated. As illustrated in Fig. 6, the time when the maximum relative intensity of continuum radiation appeared was kept at around 30 ns as the laser energy or gas pressure rose. Meantime, the fitted relaxation time, *i.e.*, when the intensity was reduced to 1/*e* of the peak, are also displayed, and it can be seen that it changed little as the laser energy rose, while it showed a decreasing trend with greater gas pressure due to the more frequent collisions caused by there being more particles. If the practical application requires higher pressure, the relaxation time would get shorter with less possibility of ignition. In addition, the relaxation time changed with pressure linearly so that a predictive value could be obtained for other conditions. Determination of the ignition state with a flammable sample based on LIBS is a necessary step before setting up the experiment, as described in the following.

3.2 Temporal characteristics of atomic spectral lines

The spectral lines of atoms (H_α 656.3 nm, N–I 742.3 nm, 744.2 nm, 746.8 nm and O–I 777 nm) were collected by a spectrometer. A typical laser-induced breakdown spectrum of premixed ADN-based propellant/argon gas was recorded and is shown in Fig. 7. The pressure was set at 40 kPa and the mass flow rate was 2.62 g h^{-1}.

The effective lifetimes of the emission lines of H, N and O atoms were investigated by time-resolved LIBS technique to determine the suitable experimental parameters. The total pressure of gases was 70 kPa, while the gate width of ICCD was programmed as 50 ns. Delay of the ICCD was set above 500 ns to reduce the intensity of the continuum radiation. The time-resolved intensities of the spectral lines of H, N and O atoms are demonstrated in Fig. 8.

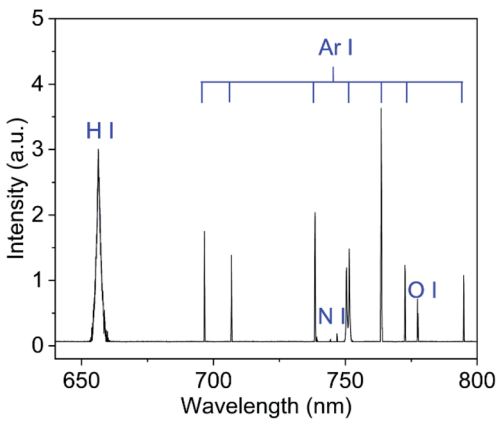

Fig. 7 Typical spectrum of premixed and-based propellant/argon gas in the LIBS experiment.

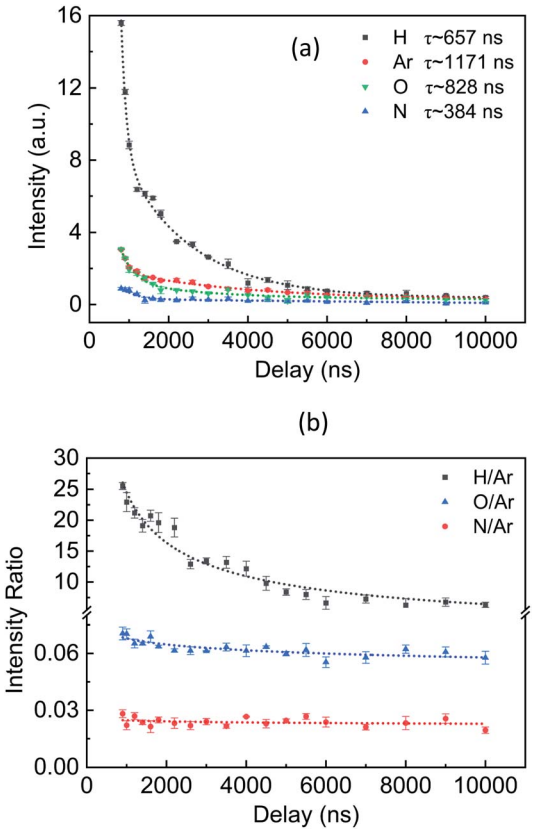

Fig. 8 Relaxation processes of the spectral lines of H, Ar, N and O atoms in terms of the: (a) absolute and (b) relative intensity.

In Fig. 8(a), the colourized dotted curves are mono-exponential fittings of four sets of data. The emission lifetimes of the spectral lines could be derived directly from the curves, which were ~657 ns for H excited atoms with an upper energy level of 3d, ~1171 ns for Ar excited atoms with an upper energy level of $3s^2 3p^5(^2P_{3/2})4p$, ~828 ns for O excited atoms with an upper energy level of $2s^2 2p^3(^4S^0)3p$, and ~384 ns for N excited atoms with an upper energy level of $2s^2 2p^3(^3P)3p$ in the present LIBS experiment. Similar results were found in the work of Camacho *et al.*[35] and Cao *et al.*[36] Obviously, the intensities of the spectral lines were too weak to be detected when the data acquisition started at 4 μs after the impacting of the laser pulse. Meantime, the variation of the relative intensities of the atomic spectral lines were considered carefully while the decay processes of the relative intensities of the spectral lines were also investigated, as shown in Fig. 8(b). The decrease trend of the relative intensity ratio was mainly due to the lower concentration of N, H and O compared with Ar, which led to a steeper reduction of the former. A better SNR (signal-to-noise ratio) was observed with a delay greater than 1.6 μs according to

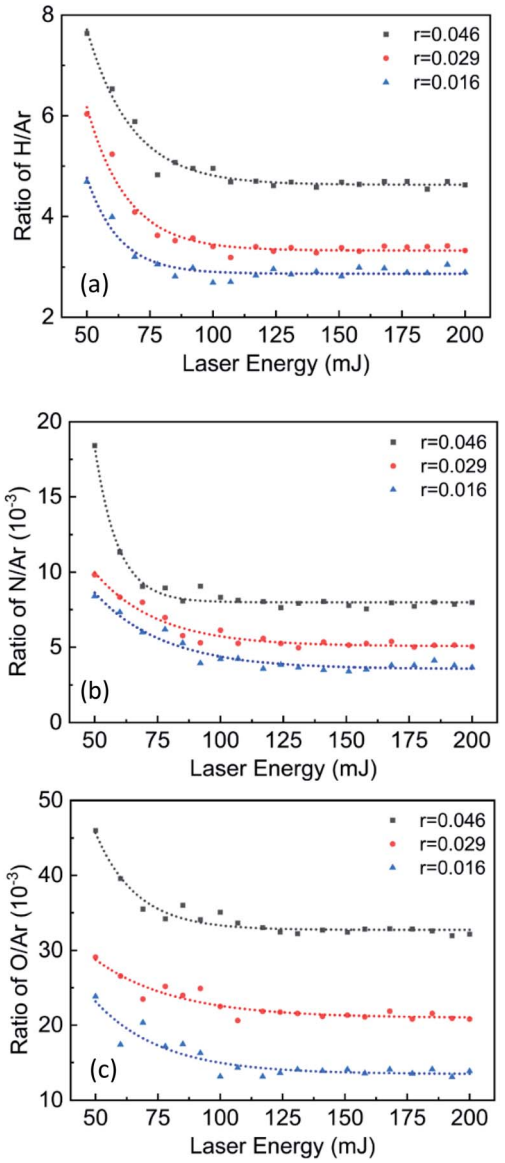

Fig. 9 Relative intensity ratios of the atomic emission lines of (a) H/Ar (b) N/Ar (c) O/Ar as a function of the laser pulse energy for premixed ADN-based propellant/argon gas.

Fig. 3. Furthermore, the relative intensity ratios were almost constant above 2 μs. The delay was thus set above 2 μs to avoid the oscillation of the intensity ratio and as this would not affect the equivalence ratio measurement. Combined with the lifetime of each atom, the time window was set in the region from 2 μs to 4 μs in the current LIBS set-up to maximize the SNR and minimize the data jitter.

3.3 Effect of laser energy on the intensity ratio

In the LIBS technique, the temperature of the laser-induced local plasma must be hot enough to dissociate the target molecules into their constituent atoms. The right value of excited energy for a specific molecule should be higher than its "saturation threshold", which is defined as the initiation point of the intensity ratio in the relatively stationary region. The variation of the intensity ratio is affected by the concentration of the detected species, the plasma size, and the settings of the diagnostic system, *etc.* In order to explore the effect of the laser energy on the intensities of the spectral lines, the above-mentioned variables were controlled under the same conditions in the current experiment. The energy of the excited laser was in the range of 50–200 mJ per pulse and the total gas pressure was fixed at 70 kPa. As shown in Fig. 9, the saturation threshold of ADN/Ar, which is presented as inflection point of the curve, was investigated based on the relative intensities of H/Ar, N/Ar, O/Ar with three different mixture ratios. Note that the signal intensities were calculated by the peak area of the spectra.

It is suggested that the mixture in the probe volume displays a saturation phenomenon when the laser energy is over 120 mJ per pulse in Fig. 9. The values of H/Ar, N/Ar, O/Ar of the three mixture ratios changed little within the laser energy from 120–200 mJ per pulse. Therefore, the excited laser energy of a single pulse was set as 140 mJ with a gate delay and width of 2 μs and 1 μs in the present work. This arrangement makes the LIBS signal strong enough as well as keeps it apart from the continuum emission of the luminous plasma. The specific value of the saturation threshold is related to the experimental conditions as discussed previously. Therefore, it is worth noting that the saturation threshold increased by 20% as the gas pressure rose to 100 kPa on account of the greater gas pressure leading to a higher saturation threshold.

Despite the specific value related to the experimental conditions, the production rate of different atoms could be inferred from the trend of the saturation threshold. In Fig. 9, the ratios of H/Ar, N/Ar, O/Ar decreased with the excited energy as represented by the increase in H or N or O atomic emission intensity gradually lagging behind the growth of Ar as the laser energy was increased. Alongside the laser energy, the effect of the mixture ratio on the saturation threshold was also investigated. The transition energy from high to low of the emission spectral lines in the present experiment followed the order: $H_{656.3\ nm} > Ar_{738.4\ nm} > N_{746.8\ nm} > O_{777\ nm}$. In the volume of the laser-induced plasma, atoms with a lower transition energy have a greater odds of being excited. A greater mixture ratio translates to a relative larger concentration of H, N and O atoms and a relative lower concentration of Ar atoms. This means that when the mixture ratio increased, an increment of laser energy was necessary to accomplish the photoexcitation process of the H atoms and the excitation for Ar atoms, which led to the saturation threshold of H/Ar growing, as seen in Fig. 9(a). However, N/Ar and O/Ar acted in an opposite way, as seen in Fig. 9(b) and (c), for the same reason that indicated that the increment of the relative concentration of the atomic species had a great impact on the emission intensity. As a result, the aforementioned trend can be utilized to infer the saturation threshold with a certain state.

3.4 Linear correlation between the emission intensity ratio and the mixture ratio

The emission intensity ratio of spectral peaks is correlated with the relative concentration of the elemental composition at

a given mixture ratio condition. There can be some inherent variability uncertainties associated with experimental repetitions, especially due to uncertainties associated with the mixture ratio measurements. However, it is clear that the intensity ratio trends diminish the influence of these sources of variability. The relationship between the value of the relative intensity and the mixture ratio was measured in this chamber at different pressures to simulate the microthruster combustion state.

Here, the single pulse energy of excited laser was fixed at 140 mJ. The LIBS emission of atoms was focused into the fibre and transmitted into the spectrometer with a delay and width of 2 μs and 1 μs, respectively. The mixture ratio was in the range of 0–0.06 and the pressure of the chamber was varied at 40, 55, 70, 85 and 100 kPa. The linear correlations between the emission intensity ratio and the mixture ratio under different pressures are presented in Fig. 10.

It was clearly shown that the lower the gas pressure, the greater the slopes of the linear correlations, no matter whether for H/Ar or N/Ar or O/Ar. In LIBS measurement, R^2 (goodness of fit) is an important index for the linear correlation between the mixture ratio and intensity ratio, and is used for assessing the calibration model established from similar experiments.[37,38] Fig. 10 shows that the R^2 values of 15 fitted curves were greater than 0.96 mostly. It is important to compare the slope since a higher slope indicates a higher sensitivity; therefore it is important to ensure that the intensity ratio calibration exhibits a higher sensitivity to variations in the mixture ratio to facilitate its use as a detection tool. With Fig. 10, it can be concluded that the H/Ar intensity ratio calibration was a better choice to measure the mixture ratio compared to N/Ar and O/Ar. Moreover, the linear correlation could be extendable to other working conditions as long as the emission spectral lines could be detected. Taking a previous work carried out by Wada *et al.*[39] as an example, where the electric ignition characteristics of an ADN-based propellant were studied based on the discharge plasma, the mass flow of ADN-based propellant was 0.637 g s^{-1} with in an undersea level and in a vacuum condition, which could be evaluated by the extension of the curve in Fig. 10.

More intuitive results can be deduced from Fig. 10 and display the relationship between the slopes and gas pressures of the discharge chamber in Fig. 11. The slope of the calibration lines decreased with the pressure in the present LIBS experiment, which was due to the particle densities as well as the interactions increasing with the pressure. The quenching of excited atoms was also intensified greatly by the increase in pressure, while the intensities of the spectral lines were weakened. Therefore, it is believed that the reduced variation of the slopes originated from the increasing pressure.

As shown in Fig. 11, the linear correlation between the gas pressure and the logarithm of the slope can be promoted to a typical pressure region of the thruster chamber, 0.1–1 MPa usually. The mass flow of the ADN-based propellant when testing a practical thruster is much greater than the value of the current lab-scale status. Consequently, the mixture ratio region

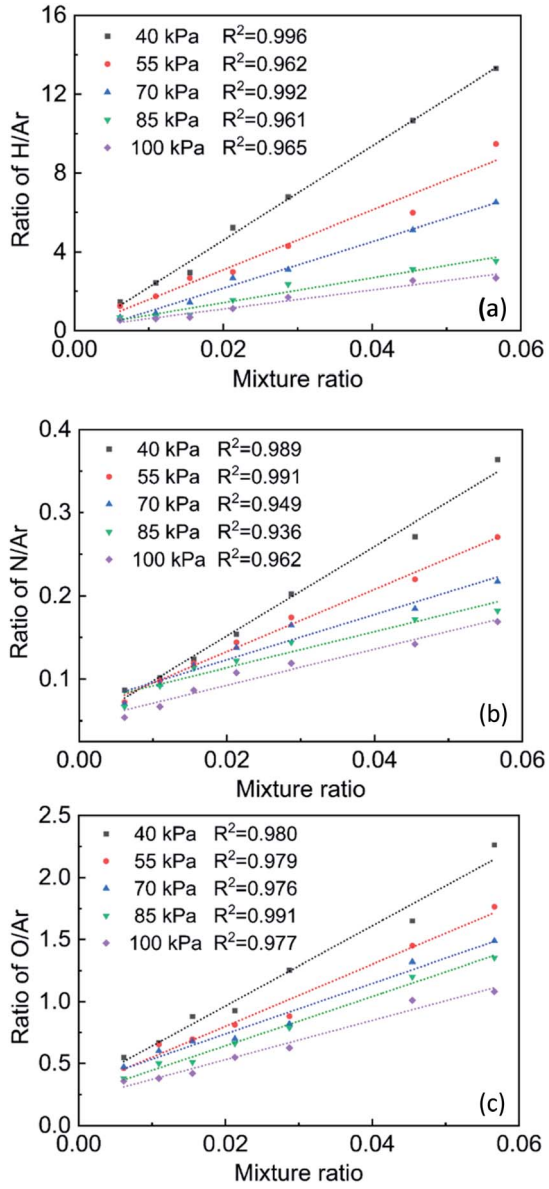

Fig. 10 Correlation of the mixture ratio with the relative intensity of the ratios of: (a) H/Ar (b) N/Ar (c) O/Ar under different pressures.

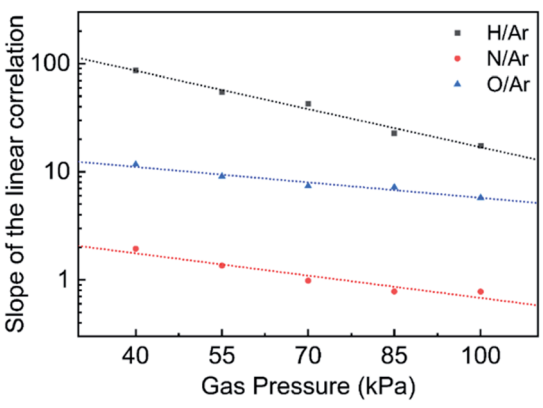

Fig. 11 Variation of the slopes of the calibration lines with the chamber pressure.

is not emphasized deliberately because it would not hinder the promotion procedure of these linear correlations shown in Fig. 10 to other working conditions.

3.5 Effect of the gas pressure on the FWMH of H and Ar

As a vital input parameter, the gas pressure should be determined to obtain the local mixture ratio based on the linear correlation in the previous section. Obtaining information on the gas pressure from the spectra directly would be a significant step in the process of performing *in situ* measurements. It is known that the confinement effect of ambient gas on plasma increases as the gas pressure rises, which causes stronger collisions and a higher electron density. So, the widths of the spectral lines would go up for a plasma with increasing electron density. The FWHM of the observed spectral lines was a convolution result of natural broadening, instrumental broadening, Doppler broadening and Lorentzian broadening (which contains collisional broadening and stark broadening). Among this, natural and instrumental broadening were fixed by using the same experimental apparatus. Doppler broadening is in the form of a Gaussian profile, whose influence is eliminated during the deconvolution processing. Consequently, the variations of FWHM in different tests was mainly determined by the Lorentzian broadening. Furthermore, the FWHM of spectral lines varies with the gas pressure linearly according to the Stern–Vollmer equation: $\omega_{\mathrm{FWHM}} = aP + b$.

With a laser energy of 140 mJ per pulse and a mixture ratio of 0.057, the pressure dependence of FWHM of different spectral lines was determined and the results are presented in Fig. 12. Apparently, the FWHM of the spectral lines increased linearly with the pressure as described by the Stern–Vollmer equation. The curve of the H atom is applied more widely since it has a steeper slope. However, H atoms are not contained in some compounds; furthermore, H atoms have a greater chemical reactivity than inert atoms. In order to make the linear correlation more universal, a few FWHM from argon's spectral lines were also assessed, given the inert gas barely affects the chemical reactions. This means that Ar atoms that have long-lived emission spectral lines can be added to the flow field to be measured.

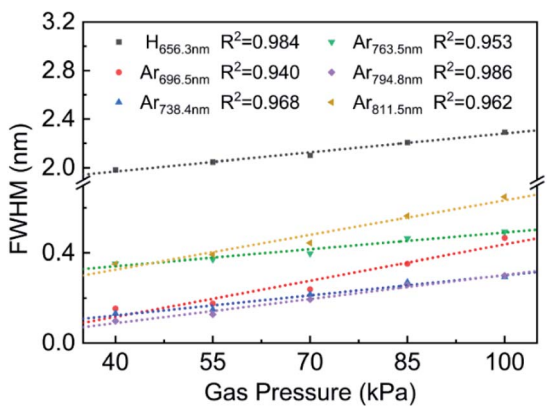

Fig. 12 Linear correlation between the full width at half maximum (FWHM) of the spectral lines with the gas pressure when the mixture ratio was 0.057.

In general, although a higher R^2 value is desirable, a greater slope is a more significant factor to ensure the intensity ratio exhibits a better sensitivity to variations in the mixture ratio. It also means that instead of the goodness of fit shown in Fig. 12, the slope should be taken into account first. As a result, it may be concluded that $Ar_{811.5\ nm}$ with a greater slope of 0.0052 is a better choice to obtain the local pressure in more common cases.

Here, a procedure of applying the LIBS technique to diagnose the mixture ratio can be summarized as follows. First, the time window of the acquisition and laser energy have to be set to reasonable values according to Sections 3.2 and 3.3. Then, the local pressure is analysed from the FWHM of the spectral lines discussed in Section 3.5 as an essential precondition to obtain the mixture ratio. The intensity ratios of the spectral lines are obtained with further analysis of the spectra. Under a certain pressure, the mixture ratio can also be determined based on the linear correlation formula from Section 3.4. Note that when the gas pressure and intensity ratio are not in the range mentioned above, it could still refer to the extended line discussed in Section 3.4.

4. Conclusions

The current study mainly focused on the quantitative measurement of the mixture ratio with a premixed ADN-based propellant/argon gas mixture under simulated space propulsion conditions. Both ultrahigh-speed imaging and laser-induced breakdown spectroscopy (LIBS) were used to study the state of the laser-induced plasma. It is desirable and important to establish a linear correlation between the mixture ratio within 0–0.06 and the relative intensity ratios for hydrogen (656.3 nm)/nitrogen (746.8 nm)/oxygen (777 nm) to argon (738.4 nm) under a gas pressure from 40 kPa to 100 kPa. The salient conclusions drawn from this work are as follow:

(1) Continuum radiation and effective lifetimes were studied to determine the acquisition time window of LIBS. It was observed that the intensities of the continuum radiation would not interfere with the LIBS signal till the delay at around 1 μs. Hence a time window with a better SNR was defined combining the effective lifetimes of the spectral lines.

(2) For the reliability of the data obtained from LIBS, the impact of the laser energy on the emission ratio of the spectral lines were investigated to figure out the saturation threshold. Besides, it was evidenced that the transition energy of each atom was related to the sequence of its production rate.

(3) The correlations between the mixture ratio of the propellant/Ar and intensity ratio of H/Ar, O/Ar, N/Ar were obtained and linearly fitted. The slopes of the fitted lines decreased with the increase in the chamber pressure due to the particle densities and the interactions were all increased, while the quenching of the excited atoms was also intensified greatly in the present LIBS experiment.

(4) For prediction of an unknown dataset, the mixture ratio was better obtained from the H/Ar calibration than from O/Ar or

N/Ar due to the higher sensitivity; that is, the greater slope of the fitted lines.

(5) Determination of the pressure value was a prerequisite for applying the linear correlation between the emission ratio and mixture ratio. Considering the pressure dependence of FWHM of the spectral lines, it was found that in addition to the traditional FWHM of the $H_{656.3\ nm}$ atom, $Ar_{811.5\ nm}$ was also a good choice to infer the pressure with an improved universality.

To sum up, the fundamental data obtained here could be a reference for the on-line quantitative measurements of mixture ratios with ADN-based propellants, which is of great interest for better understanding the detailed kinetics. Besides, exploring the distribution state of ADN-based propellants by LIBS allows great convenience to make targeted improvements in the propulsion efficiency for further studies.

Author contributions

Fangyi Wang: Conceptualization, Methodology, Data curation, Software, Formal analysis, Investigation, Writing – original draft, Writing – review & editing. Shaohua Zhang: Conceptualization, Formal analysis, Supervision, Writing – review & editing, Resources, Funding acquisition. Xilong Yu: Conceptualization, Project administration, Funding acquisition. Xin Lin: Investigation, Validation. Jing Li: Investigation, Software. Yan Liu: Investigation, Funding acquisition.

Conflicts of interest

There are no conflicts to declare.

Acknowledgements

The work is partially supported by the National Science Foundation of China (grant no. 11672359, 11872368, 11927803) and Natural Science Foundation of Beijing Municipality (grant no. BM2019001).

Notes and references

1 H. Östmark, U. Bemm, A. Langlet, R. Sandén and N. Wingborg, The properties of ammonium dinitramide (ADN): Part 1, basic properties and spectroscopic data, *J. Energ. Mater.*, 2000, **18**(2–3), 123–138.

2 A. Hahma, H. Edvinsson and H. Östmark, The Properties of Ammonium Dinitramine (ADN): Part 2: Melt Casting, *J. Energ. Mater.*, 2010, **28**(2), 114–138.

3 K. Anflo and B. Crowe, *In-Space Demonstration of an ADN-based Propulsion System*, 2011.

4 Y. Batonneau, R. Brahmi, B. Cartoixa, K. Farhat, C. Kappenstein, S. Keav, G. Kharchafi-Farhat, L. Pirault-Roy, M. Saouabé and C. Scharlemann, Green Propulsion: Catalysts for the European FP7 Project GRASP, *Top. Catal.*, 2013, **57**(6–9), 656–667.

5 M. Negri, M. Wilhelm and C. Hendrich, *Development of ADN-based Thruster Technologies – An overview of the European Project Rheform*, 2018.

6 R. Pflieger, M. Lejeune, C. Noel, T. Belmonte, S. I. Nikitenko and M. Draye, Diagnosing the plasma formed during acoustic cavitation in [BEPip][NTf2] ionic liquid, *Phys. Chem. Chem. Phys.*, 2019, **21**(3), 1183–1189.

7 A. Starikovskiy and N. Aleksandrov, *Plasma-Assisted Ignition and Combustion*, 2011.

8 K. S. Koh, J. Chin and T. F. Wahida Ku Chik, Role of electrodes in ambient electrolytic decomposition of hydroxylammonium nitrate (HAN) solutions, *Propuls. Power Res.*, 2013, **2**(3), 194–200.

9 P. Khare, V. Yang, H. Meng, G. A. Risha and R. A. Yetter, Thermal and Electrolytic Decomposition and Ignition of HAN–Water Solutions, *Combust. Sci. Technol.*, 2015, **187**(7), 1065–1078.

10 T. Ono, T. Segawa, N. Saito, E. Takahashi and M. Nishioka, Effect of Long-Lived Species Generated by Non-Thermal Plasmas on the Auto-Ignition Delay of Liquid Hydrocarbon Fuel-Air Pre-Mixtures, *Combust. Sci. Technol.*, 2017, **189**(9), 1624–1638.

11 F. Anabitarte, A. Cobo and J. M. Lopez-Higuera, Laser-Induced Breakdown Spectroscopy: Fundamentals, Applications, and Challenges, *ISRN Spectrosc.*, 2012, **2012**, 285240.

12 S. N. Thakur and J. P. Singh, *Fundamentals of LIBS and recent developments*, 2020, pp. 3–22.

13 D. M. Surmick and C. G. Parigger, Time-resolved aluminium laser-induced plasma temperature measurements, *J. Phys.: Conf. Ser.*, 2014, **548**, 012046.

14 D. W. Hahn and N. Omenetto, Laser-Induced Breakdown Spectroscopy (LIBS), Part II: Review of Instrumental and Methodological Approaches to Material Analysis and Applications to Different Fields, *Appl. Spectrosc.*, 2012, **66**(4), 347–419.

15 J. Laserna, J. M. Vadillo and P. Purohit, Laser-Induced Breakdown Spectroscopy (LIBS): Fast, Effective, and Agile Leading Edge Analytical Technology, *Appl. Spectrosc.*, 2018, **72**(1), 35–50.

16 A. K. Patnaik, P. S. Hsu, A. J. Stolt, J. Estevadeordal, J. R. Gord and S. Roy, *Advantages of Ultrafast LIBS for High-Pressure Diagnostics*, 2018, LW5C.4.

17 S. Zhang, X. Yu, F. Li, G. Kang, L. Chen and X. Zhang, Laser induced breakdown spectroscopy for local equivalence ratio measurement of kerosene/air mixture at elevated pressure, *Opt Laser. Eng.*, 2012, **50**(6), 877–882.

18 L. Merotto, M. Sirignano, M. Commodo, A. D'Anna, F. Migliorini, R. Dondè and S. De Iuliis, Probing the equivalence ratio in partially premixed flames by combining optical techniques and modeling results, *Combust. Sci. Technol.*, 2018, **190**(8), 1442–1454.

19 S. G. Buckley, F. Ferioli and G. A. Lithgow, *Combustion system analysis using laser-induced breakdown spectroscopy*, 2003, p. 403.

20 T. Badawy, M. Hamza, M. S. Mansour, A.-H. H. Abdel-Hafez, H. Imam, M. A. Abdel-Raheem, C. Wang and T. Lattimore, Lean partially premixed turbulent flame equivalence ratio measurements using laser-induced breakdown spectroscopy, *Fuel*, 2019, **237**, 320–334.

21 P. Stavropoulos, A. Michalakou, G. Skevis and S. Couris, Quantitative local equivalence ratio determination in laminar premixed methane–air flames by laser induced breakdown spectroscopy (LIBS), *Chem. Phys. Lett.*, 2005, **404**(4–6), 309–314.
22 A. H. Rezaei, M. H. Keshavarz, M. K. Tehrani and S. M. R. Darbani, Quantitative analysis for the determination of aluminum percentage and detonation performance of aluminized plastic bonded explosives by laser-induced breakdown spectroscopy, *Laser Phys.*, 2018, **28**(6), 065605.
23 P. Monkhouse, On-line spectroscopic and spectrometric methods for the determination of metal species in industrial processes, *Prog. Energy Combust. Sci.*, 2011, **37**(2), 125–171.
24 J. L. Gottfried, *Laser-induced air shock from energetic materials (LASEM) method for estimating detonation performance: Challenges, successes and limitations*, 2018, vol. 1979, p. 100014.
25 M. O'Neil, N. A. Niemiec, A. R. Demko, E. L. Petersen and W. D. Kulatilaka, Laser-induced-breakdown-spectroscopy-based detection of metal particles released into the air during combustion of solid propellants, *Appl. Opt.*, 2018, **57**(8), 1910–1917.
26 A. H. Farhadian, M. K. Tehrani, M. H. Keshavarz, M. Karimi and S. M. Reza Darbani, Relationship between the results of laser-induced breakdown spectroscopy and dynamical mechanical analysis in composite solid propellants during their aging, *Appl. Opt.*, 2016, **55**(16), 4362–4369.
27 A. H. Farhadian, M. K. Tehrani, M. H. Keshavarz, M. Karimi, S. M. R. Darbani and A. H. Rezayi, A novel approach for investigation of chemical aging in composite propellants through laser-induced breakdown spectroscopy (LIBS), *J. Therm. Anal. Calorim.*, 2015, **124**(1), 279–286.
28 C. R. Bhatt, C. L. Goueguel, J. C. Jain, D. L. McIntyre and J. P. Singh, *LIBS application to liquid samples*, 2020, pp. 231–246.
29 S. J. Mousavi, M. Hemati Farsani, S. M. R. Darbani, N. Asadorian, M. Soltanolkotabi and A. Eslami Majd, Identification of atomic lines and molecular bands of benzene and carbon disulfide liquids by using LIBS, *Appl. Opt.*, 2015, **54**(7), 1713.
30 H. Nozari, F. Rezaei and S. H. Tavassoli, Analysis of organic vapors with laser induced breakdown spectroscopy, *Phys. Plasmas*, 2015, **22**(9), 093302.
31 R. Stützer, M. Börner, M. Kuchelmeister and M. Oschwald, *Laser-Induced Breakdown Spectroscopy on Gas Compositions for Equivalence Ratio Determination in Space Propulsion*, Space Propulsion, Rome, Italy, 2016.
32 S. H. Lee, H. Do and J. J. Yoh, Simultaneous optical ignition and spectroscopy of a two-phase spray flame, *Combust. Flame*, 2016, **165**, 334–345.
33 P. D. Gupta, P. A. Naik and H. C. Pant, Effect of recombination on ion expansion velocity in laser-produced plasmas, *J. Appl. Phys.*, 1984, **55**(3), 701–703.
34 G. Befki, *Radiation processes in plasmas*, Wiley Series in Plasma Physics, 1966.
35 J. J. Camacho, M. Oujja, M. Sanz, A. Martínez-Hernández, I. Lopez-Quintas, R. de Nalda and M. Castillejo, Imaging spectroscopy of Ag plasmas produced by infrared nanosecond laser ablation, *J. Anal. At. Spectrom.*, 2019, **34**(3), 489–497.
36 Y. Cao, X.-L. Liu, W.-D. Xian, S.-H. Sun, M.-Z. Sun, P.-J. Ding, Y. C. Shi, Z.-Y. Liu and B.-T. Hu, Characterization of Femtosecond Laser-Induced Plasma under Low Pressure in Argon, *Chin. Phys. Lett.*, 2015, **32**(3), 035203.
37 S. Sheta, M. S. Afgan, Z. Hou, S.-C. Yao, L. Zhang, Z. Li and Z. Wang, Coal analysis by laser-induced breakdown spectroscopy: a tutorial review, *J. Anal. At. Spectrom.*, 2019, **34**(6), 1047–1082.
38 M. M. Tripathi, K. K. Srinivasan, S. R. Krishnan, F.-Y. Yueh and J. P. Singh, A comparison of multivariate LIBS and chemiluminescence-based local equivalence ratio measurements in premixed atmospheric methane–air flames, *Fuel*, 2013, **106**, 318–326.
39 A. Wada and H. Habu, *Electric Ignition Characteristics of an Ammonium-Dinitramide-Based Ionic Liquid Monopropellant with Discharge Plasma*, 2020.

